iScience

CellPress
OPEN ACCESS

Article

Analysis of age-related left ventricular collagen remodeling in living donors: Implications in arrhythmogenesis

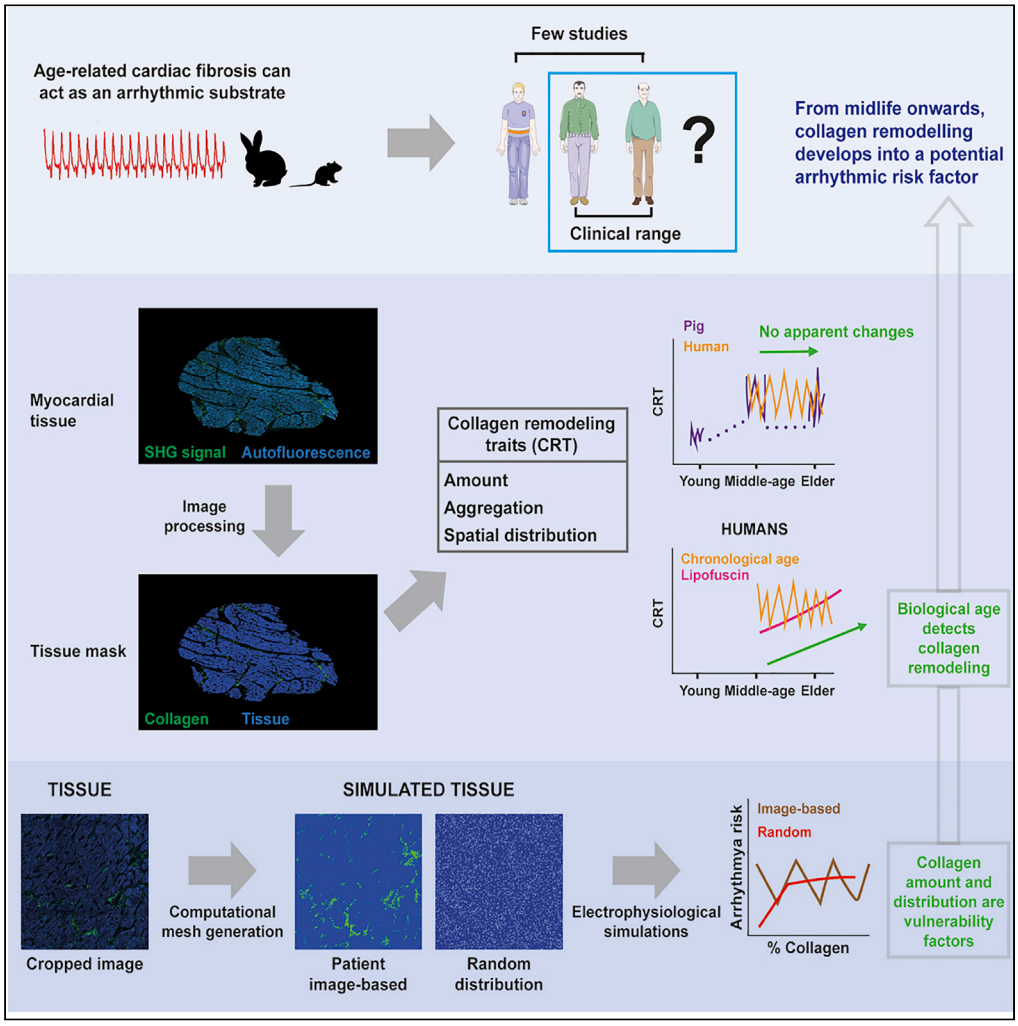

Laura García-Mendívil, María Pérez-Zabalza, Konstantinos Mountris, ..., Emiliano Diez, Laura Ordovás, Esther Pueyo

lgmendivil@unizar.es (L.G.-M.)
lordovas@unizar.es (L.O.)

Highlights

Collagen remodeling traits change from youth to adulthood, not from midlife onwards

In humans, collagen remodeling traits relate with the biological age-pigment lipofuscin

Beyond collagen amount, its distribution also influences ventricular arrhythmogenesis

Consistent age-related remodeling was observed amid healthy farm pigs and living donors

García-Mendívil et al., iScience 25, 103822
February 18, 2022 © 2022 The Author(s).
https://doi.org/10.1016/j.isci.2022.103822

iScience

CellPress
OPEN ACCESS

Article

Analysis of age-related left ventricular collagen remodeling in living donors: Implications in arrhythmogenesis

Laura García-Mendívil,[1,2,*] María Pérez-Zabalza,[1,2] Konstantinos Mountris,[1,2] Sam Duwé,[3] Nick Smisdom,[4] Marta Pérez,[5,6] Lluís Luján,[6,7] Esther Wolfs,[4] Ronald B. Driesen,[4] José María Vallejo-Gil,[8] Pedro Carlos Fresneda-Roldán,[8] Javier Fañanás-Mastral,[8] Manuel Vázquez-Sancho,[8] Marta Matamala-Adell,[8] Juan Fernando Sorribas-Berjón,[8] Javier André Bellido-Morales,[8] Francisco Javier Mancebón-Sierra,[8] Alexánder Sebastián Vaca-Núñez,[8] Carlos Ballester-Cuenca,[8] Aida Oliván-Viguera,[1,2,9] Emiliano Diez,[10] Laura Ordovás,[1,2,11,12,*] and Esther Pueyo[1,2,9]

SUMMARY

Age-related fibrosis in the left ventricle (LV) has been mainly studied in animals by assessing collagen content. Using second-harmonic generation microscopy and image processing, we evaluated amount, aggregation and spatial distribution of LV collagen in young to old pigs, and middle-age and elder living donors. All collagen features increased when comparing adult and old pigs with young ones, but not when comparing adult with old pigs or middle-age with elder individuals. Remarkably, all collagen parameters strongly correlated with lipofuscin, a biological age marker, in humans. By building patient-specific models of human ventricular tissue electrophysiology, we confirmed that amount and organization of fibrosis modulated arrhythmia vulnerability, and that distribution should be accounted for arrhythmia risk assessment. In conclusion, we characterize the age-associated changes in LV collagen and its potential implications for ventricular arrhythmia development. Consistency between pig and human results substantiate the pig as a relevant model of age-related LV collagen dynamics.

INTRODUCTION

Age-induced accumulation of myocardial interstitial fibrosis leads to cardiac mechanical and electrical dysfunction and is commonly associated with cardiovascular diseases, the foremost cause of death worldwide (Biernacka and Frangogiannis, 2011; Burlew and Weber, 2002). The extracellular matrix is a key component of the myocardium that contributes to its biomechanical behavior. Within the protein network, collagen fibrils are principal constituents that provide support to the contractile machinery. From animal studies, it is known that while collagen helps to maintain myocardial structure in healthy young hearts, the increased collagen content in aged hearts, together with additional age-related cardiac remodeling, reduces cell-to-cell coupling and impedes normal electrical propagation, facilitating arrhythmias (de Jong et al., 2011; Suk et al., 2008). Not only the amount of collagen, but also its spatial distribution and architecture play a role in impulse conduction and arrhythmogenesis (de Bakker et al., 1993; de Jong et al., 2011; Kawara et al., 2001; Kazbanov et al., 2016).

In human hearts, macroscopic fibrosis is evaluated *in vivo* mainly by non-invasive cardiac MRI (CMRI) (Suk et al., 2008). Strong dependence of magnetic resonance fibrosis markers on age (Liu et al., 2013) and correlation with ventricular arrhythmias and sudden cardiac death (Disertori et al., 2017) has been reported. However, CMRI and other non-invasive methods do not possess cellular or subcellular resolution (Hassan et al., 2020). The lack of microscopic definition hinders structural investigations at the histological level that could provide insight into fibrosis-related arrhythmogenic mechanisms. Histological evaluation of collagen is commonly performed by immune detection or histochemical procedures, like Masson's trichrome or Picrosirius red staining, but these techniques can disrupt the collagen fibrils and thus hamper structural analysis. Also, the automatic quantitative analysis can be affected by the variability that the staining procedures can introduce on the color balance of the

[1]Biomedical Signal Interpretation and Computational Simulation Group (BSICoS), Aragón Institute of Engineering Research, University of Zaragoza, Zaragoza 50018, Spain

[2]BSICoS, IIS Aragón, Zaragoza 50018, Spain

[3]Advanced Optical Microscopy Centre, Biomedical Research Institute, Hasselt University, Diepenbeek 3500, Belgium

[4]Biomedical Research Institute, Hasselt University, Diepenbeek 3500, Belgium

[5]Department of Anatomy, Embryology and Animal Genetics, University of Zaragoza, Zaragoza 50013, Spain

[6]Instituto Universitario de Investigación Mixto Agroalimentario de Aragón (IA2), University of Zaragoza, Zaragoza 50013, Spain

[7]Department of Animal Pathology, University of Zaragoza, Zaragoza 50013, Spain

[8]Department of Cardiovascular Surgery, University Hospital Miguel Servet, Zaragoza 50009, Spain

[9]Biomedical Research Networking Center in Bioengineering, Biomaterials and Nanomedicine (CIBER-BBN), Zaragoza 50018, Spain

[10]Institute of Experimental Medicine and Biology of Cuyo (IMBECU), CONICET, Mendoza 5500, Argentina

Continued

This is an open access article under the CC BY-NC-ND license (http://creativecommons.org/licenses/by-nc-nd/4.0/).

staining due to technical issues such as changes in the chemical formulations of the stains or the protocol used for sample fixation and storage.

Fibrillar collagen is non-centrosymmetric and has a remarkable non-linear potential, thus being capable of generating very bright second harmonics. Second-harmonic generation (SHG) microscopy exploits this property to specifically investigate the collagen matrix in different tissues. SHG microscopy has a label-free nature (Mostaço-Guidolin et al., 2017) that, besides providing highly specific signal, it is an interesting feature when tissue samples are scarce, as those from human LV biopsies from living donors, as it does not consume sample. Also, it has submicron resolution (Williams et al., 2005), which enables structural analysis of collagen organization, rather than just amount quantification. Assessment of collagen deposition in the human heart by SHG microscopy has been mostly evaluated from atrial tissues (Büttner et al., 2018; Tsai et al., 2010), while information from the human LV is scant (Perbellini et al., 2017, 2018). In addition to the described SHG characteristics, its specificity and resolution enable the development of precise methods for (semi-)automatic quantification (Chiu et al., 2010; Liu et al., 2017). Currently employed methods for fibrosis characterization from SHG images study mainly collagen fiber alignment and the degree of isotropy (Ávila and Bueno, 2015; Liu et al., 2017; Tsai et al., 2010). A few works in the literature also characterize its spatial distribution (Strupler et al., 2007; Tilbury et al., 2014), but as far as we know none of them in relation to myocardial fibrosis.

To the best of our knowledge, the amount of age-related collagen deposition in the human LV has been analyzed in very few studies using standard histochemical techniques (Gazoti Debessa et al., 2001; Mendes et al., 2012). Comparisons were carried out between young (twenties) and elder (from sixties to eighties) individuals, thus leaving unresolved the age ranges of clinical relevance related to increased arrhythmic risk (Segovia-Roldan et al., 2021). In addition, such studies disregard collagen organization. In agreement with their results, we recently confirmed the age-related increase in total LV fibrosis in comparable age ranges (Ramos-Marquès et al., 2021). Our results suggested that accounting for the aging rate by transcriptomic biological age better explained the increased fibrosis as compared to chronological age. Thus, histological biological age could also yield a more precise understanding of the dynamics of collagen deposition in the aging human LV. This is of special interest from midlife onwards, where changes in fibrosis could be expected to be more variable and clinically relevant than in youth, given the cumulative action of genetics and/or environment over time. Detection of increased fibrosis during middle age could be critical for early application of anti-fibrotic therapies, even at stages of subclinical evidence, as a strategy to prevent fibrosis-related ventricular arrhythmias and sudden cardiac deaths. Further studies on collagen deposition from middle age onwards are needed. Also, characterization of age-related LV myocardial fibrosis as an arrhythmogenic substrate has been mostly studied in animal models (Comtois and Nattel, 2011) or using numerical methods to simulate general fibrosis characteristics (Kazbanov et al., 2016), but not using patient-specific models representative of cardiac tissue images.

Here, transmural LV tissue sections from young, adult, and old pigs as well as middle-age to elder humans are analyzed by SHG microscopy. An automated method is developed to quantify the amount, aggregation and spatial distribution of collagen, the two latter ones based on a new variable to measure collagen assembly. To account for the fact that the aging rate highly varies among individuals, we evaluate these three features not only as a function of chronological age, but also in relation to the amount of the aging pigment lipofuscin (Kakimoto et al., 2019). We subsequently introduce the results from the experimental collagen characterization into two-dimensional computational models of human LV electrophysiology, and we assess the impact of collagen characteristics in electrical propagation and pro-arrhythmicity, obtaining improved assessment of the effect of fibrosis as a substrate for cardiac arrhythmia generation. By using the proposed multidisciplinary approach, our work demonstrates age-related changes in collagen matrix in porcine and human LV. This collagen increase is better explained by biological age than by chronological age in middle-age to elder humans and is accompanied by enhanced arrhythmia vulnerability.

RESULTS

Age alters the amount, aggregation and spatial distribution of collagen in pig LV tissue

The image processing procedure developed to evaluate collagen from SHG microscopy renders tissue masks that faithfully represent the outcome obtained by standard Masson trichrome staining (Figure 1).

[11]ARAID Foundation, Zaragoza 50018, Spain

[12]Lead contact

*Correspondence: lgmendivil@unizar.es (L.G.-M.), lordovas@unizar.es (L.O.)

https://doi.org/10.1016/j.isci.2022.103822

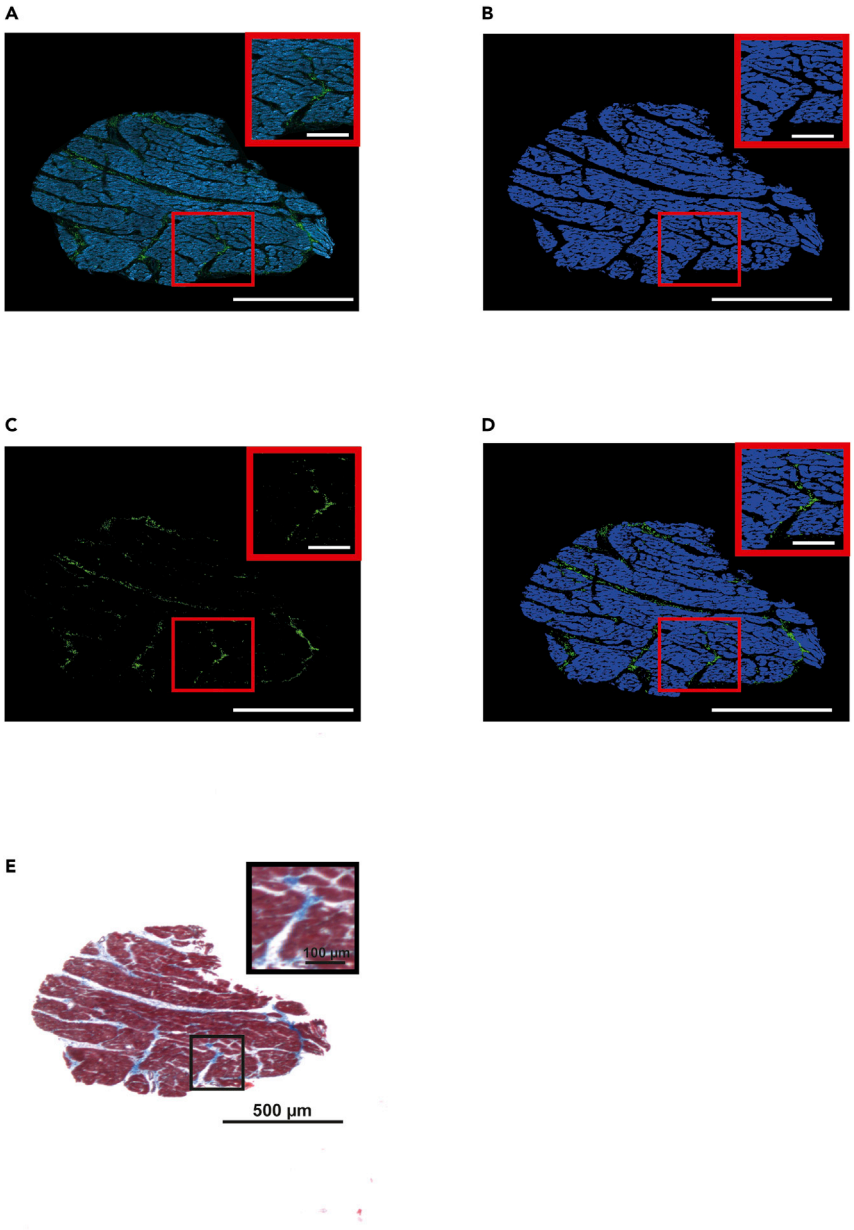

Figure 1. Collagen evaluation in SHG images using an automatic method

(A) Unprocessed SHG image (green) and autofluorescence (blue) levels of an LV tissue specimen.

(B) Extracted tissue mask obtained from the tissue autofluorescence signal.

(C) Collagen mask obtained by subtraction of autofluorescence to SHG signal.

(D) Merge of collagen (green) and tissue (blue) masks.

(E) Masson trichrome staining of a serial section of the sample shown in (A).

Evaluation of collagen characteristics by SHG in young, adult and old pigs revealed age differences in the amount of collagen (Figure 2A). These results were consistent between observers (Figure S1). In the whole set of analyzed samples, borderline significant differences in the collagen content were found between young (median [IQR]: 1.49% [1.28%–2.02%], n = 7) and old pigs (median [IQR]: 2.07% [1.79%–2.8%], n = 11), but not between adult (median [IQR]: 2.07% [1.53%–2.68%], n = 8) and old pigs. Of note, a higher degree of inter-individual variability could be observed in the old pigs, reflecting large heterogeneity in the age modulation of LV structural characteristics. Our data indicated that age increases the percentage of collagen fibrils in pig LV tissue and this is accompanied by a subtle increase in inter-individual variability.

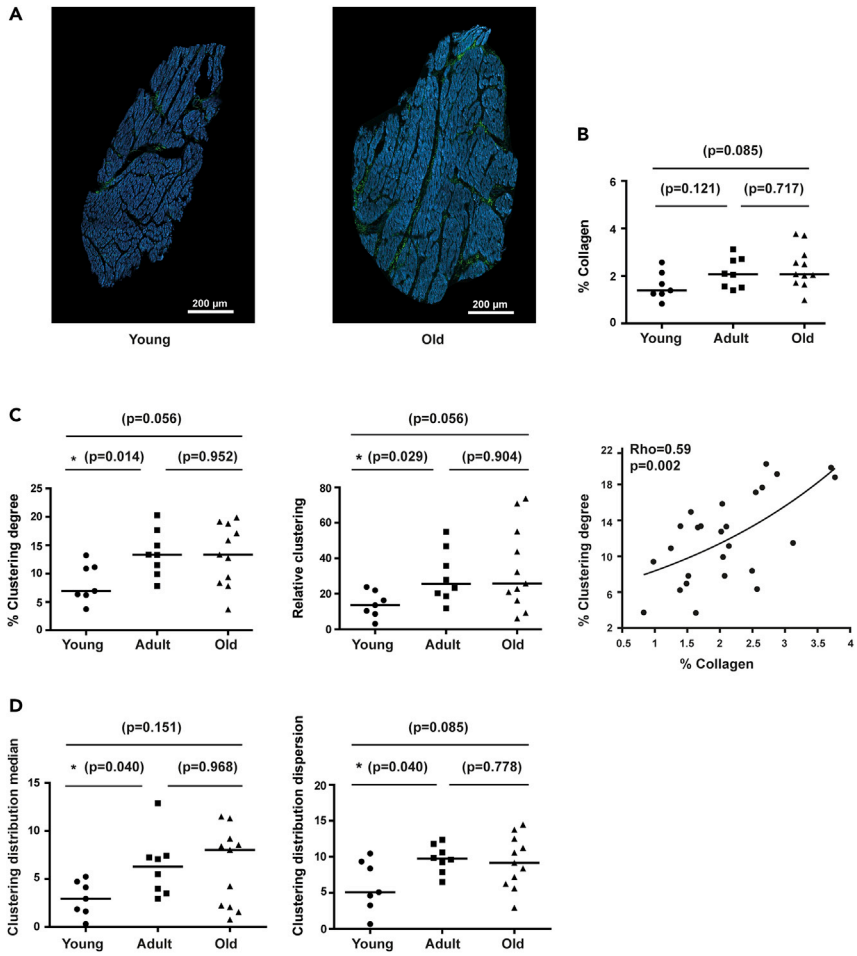

Figure 2. Quantification of collagen amount, aggregation and spatial distribution in pig LV sections

(A) Representative SHG images of LV sections from young (left) and old (right) pigs with low and high collagen content.

(B) Quantification of collagen content in young to old pigs.

(C) Quantification of clustering degree (left) and relative clustering (middle) in young, middle-age and old pigs. Correlation between collagen and clustering degree (right).

(D) Quantification of clustering distribution median (left) and clustering distribution dispersion (right) of collagen aggregations in young to old pigs.

In comparison between groups (B–D), black lines represent the median. Non-parametric Mann-Whitney test is used and p-values (p) are shown. For correlation (C), Spearman non-parametric test is used and correlation coefficients (Rho) and p-values (p) are shown. See also Figure S1

To evaluate collagen aggregation, we measured its clustering degree by quantifying the number of pixels in the collagen mask that were surrounded by a circle of collagen with a 2-pixel radius (Figure 2C). Adult pigs (median [IQR]: 13.33% [10.7%–16.3%] had significantly higher collagen clustering degree than young ones (median [IQR]: 6.95% [6.25%–11.08%], whereas differences between old (median [IQR]: 13.35% [8.63%–18.38%]) and young pigs were borderline significant (p-value = 0.056), and there were no differences between adult and old ones (p-value = 0.952). In relation to the percentage of collagen, the relative clustering was also increased (median [IQR]: 25.75‰ [17.36‰–52.26‰]) in old and adult pigs (median [IQR]: 25.57‰ [19.45‰–41.33‰] compared to young ones (median [IQR]: 13.58‰ [9.06‰–20.51‰]). The amount of collagen significantly correlated with the clustering degree (Rho = 0.59, p-value = 0.002) (Figure 2C).

To go further in the clustering evaluation, we quantified its spatial distribution by dividing every image in windows of 500 × 500 pixels and measuring the median and the dispersion of the clustering degree of all subimages (Figure 2D). Young pigs (median [IQR]: 2.93% [1.68%–4.57%] presented significantly and nearly

Table 1. Clinical characteristics of the patients

Sex	Age	Clinical history	LVEF	Ventricular hypertrophy	Dilated cardiomyopathy
Male	79	Coronary artery disease	Preserved	No	No
Male	49	Coronary artery disease	Preserved	No	No
Male	81	Coronary artery disease	Preserved	No	No
Male	50	Aortic valve stenosis	Preserved	No	No
Male	73	Coronary artery disease	Preserved	No	No
Male	60	Coronary artery disease and aortic valve stenosis	Preserved	No	No
Male	75	Coronary artery disease	Preserved	No	No
Male	63	Coronary artery disease	Preserved	No	No
Male	71	Coronary artery disease	Preserved	No	No
Male	78	Coronary artery disease	Preserved	No	No
Male	72	Coronary artery disease	Preserved	No	No
Male	58	Coronary artery disease	Preserved	No	No
Male	77	Coronary artery disease	Preserved	No	No
Male	78	Coronary artery disease	Preserved	No	No
Male	64	Coronary artery disease	Preserved	No	No
Male	57	Coronary artery disease	Preserved	No	No
Male	68	Coronary artery disease	Preserved	No	No
Male	67	Coronary artery disease	Preserved	No	No
Male	64	Coronary artery disease	Preserved	No	No
Male	62	Coronary artery disease	Preserved	No	No
Male	67	Coronary artery disease	Preserved	No	No
Male	67	Coronary artery disease	Preserved	No	No
Female	74	Coronary artery disease	Preserved	No	No
Female	61	Myxoma removal	Preserved	No	No
Female	77	Coronary artery disease	Preserved	No	No
Female	76	Coronary artery disease	Preserved	No	No

LVEF: Left ventricular ejection fraction.
A threshold of 50% was established to define preserved LVEF.

significantly lower clustering dispersion median of collagen aggregation than adult (median [IQR]: 6.27% [3.73%–7.33%]) and old pigs (median [IQR]: 8.02% [2.10%–9.03%]), respectively. A similar tendency was observed for the clustering distribution dispersion between young (median [IQR]: 5.10% (3.60%–9.10%) and adult (median [IQR]: 9.74% (8.55%–11.19%) or old pigs (median [IQR]: 9.16% (6.46%–12.18%). This indicates that young animals have less clustered collagen and a more homogeneous distribution of collagen clusters than the two older groups. No difference was observed between adults and old animals. Thus, the observed increase in clustering degree in the elder groups as compared to young animals is accompanied by a change in its spatial distribution that is not different between adult and old.

Age alters the amount, aggregation and spatial distribution of collagen in human LV tissue

Human transmural LV biopsies were collected from 26 patients from 49 to 81 years old undergoing valve replacement surgery or coronary artery bypass, having all of them preserved systolic function and absence of ventricular hypertrophy or dilated cardiomyopathy. The clinical characteristics of the patients are summarized in Table 1. Two age ranges, middle-age and elder, were considered for comparative purposes.

Alterations induced by age in the collagen characteristics of human LV tissue showed similar trends as those reported for pigs (Figure 3). Also in this case, results were comparable between observers (Figure S2).

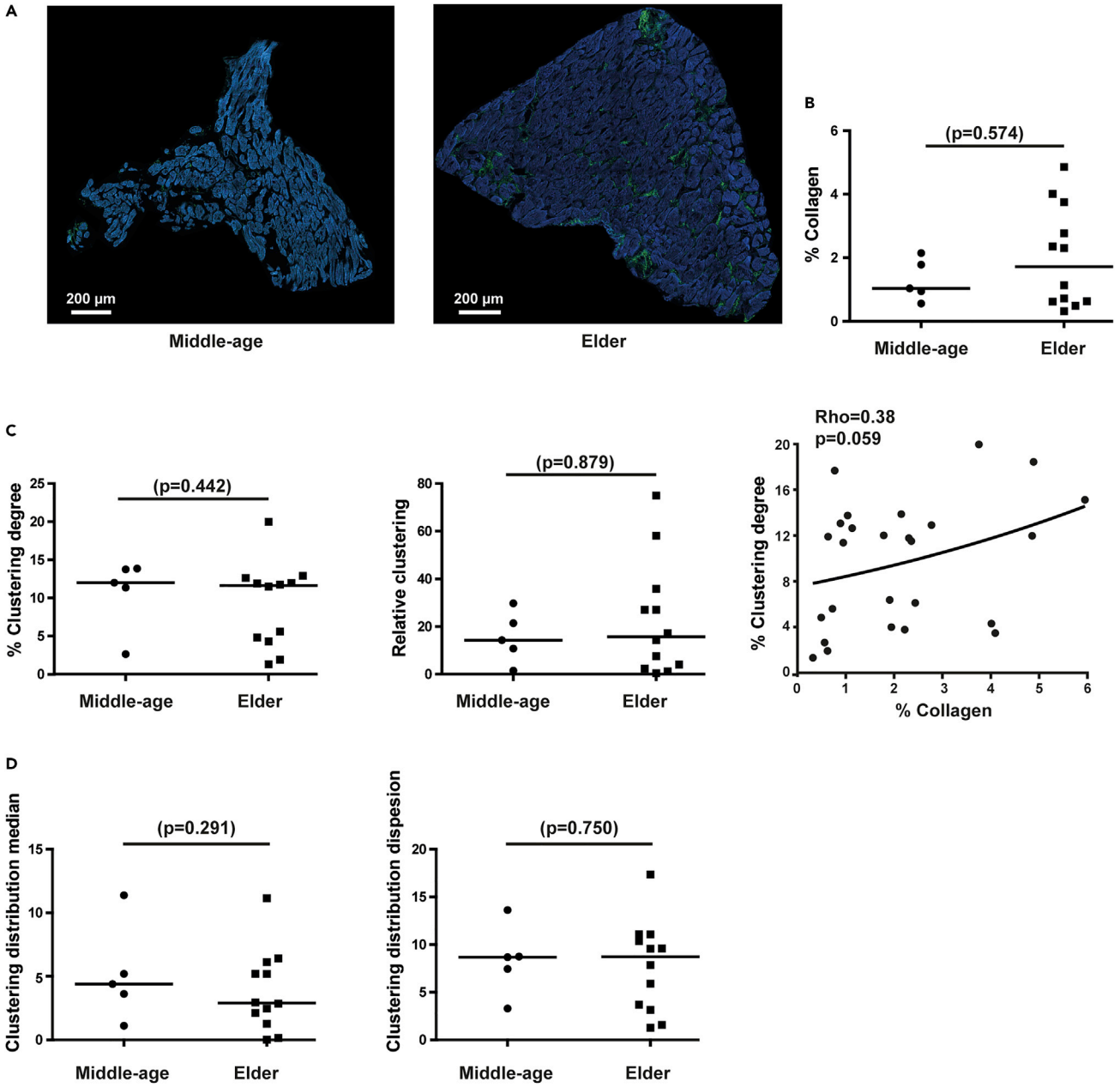

Figure 3. Quantification of collagen amount, aggregation and spatial distribution in human LV sections

(A) Representative SHG images of LV sections from middle-age (left) and elder (right) donors with low and high collagen content.

(B) Quantification of collagen content in middle-age to elder individuals.

(C) Quantification of clustering degree (left) and relative clustering (middle) in middle-age and elder individuals. Correlation between collagen and clustering degree (right).

(D) Quantification of clustering distribution median (left) and clustering distribution dispersion (right) of collagen aggregations in middle-age to elder individuals.

In comparison between groups (B–D), black lines represent the median. Non-parametric Mann-Whitney test is used and p-values (p) are shown. For correlation (C), Spearman non-parametric test is used and correlation coefficients (Rho) and p-values (p) are shown. See also Figure S2

Elder individuals had moderately higher percentages of collagen (median [IQR]: 1.72% [0.63%–3.26%], n = 12) than middle-age individuals (median [IQR]: 1.04% [0.85%–1.88%], n = 5), although differences were not statistically significant. In the elder, there was a notably higher degree of data variability than in middle-age, indicating that collagen deposition can be largely individual-dependent in this group.

The analysis of collagen aggregation showed that the percentage of clustered collagen did not vary between middle-age (median [IQR]: 12.01% [9.19%–13.78%]) and elder (median [IQR]: 11.64% [4.57%–12.31%]) individuals. A similar tendency was observed for the relative clustering between middle-age (median [IQR]: 14.28‰ [8.45‰–23.52‰]) and elder individuals (median [IQR]: 15.78‰ [3.21‰–31.47‰]). Similarly to the absolute amount of collagen, high inter-individual variability in elder was observed for both parameters (Figure 3C). Like in pigs, the increase in the percentage of collagen was accompanied by enhanced clustering degree with correlation near significance (Rho = 0.38 and p-value = 0.059) (Figure 3C).

As per the distribution of clustered collagen, the median clustering over subimages did not change significantly between middle-age (median [IQR]: 4.4% [2.99%–6.74%]) and elder groups (median [IQR]: 2.89% [1.69%–5.65%]) for the median, and a similar trend was observed for the dispersion of clustering over subimages between middle-age (median [IQR]: 8.68% [6.4%–9.96%]) and elder individuals (median [IQR]: 8.72% [3.42%–10.7%]). Thus, age did not induce evident changes in the spatial distribution of clustered collagen in the human left ventricle from midlife onwards.

Age-induced collagen alterations correlate better with lipofuscin accumulation than with chronological age in human LV tissue

Because chronological age does not necessarily reflect the structural and/or functional state of an organ, we aimed at assessing whether such degree of variability could be explained by differences in biological age, which gathers genetic and environmental factors in addition to the temporal influence of chronological age. For that purpose, we determined the content of the autofluorescent aging pigment lipofuscin (Figures 4A, 4B, and S3), obtaining similar results between observers (Figure S2). Despite the well-established relation of lipofuscin with chronological age (Brunk and Terman, 2002; Kakimoto et al., 2019), the lipofuscin content in our age groups did not differ, likely representing the high inter-individual variability in our chronological age groups, clearly observed for the collagen amount (Figure 3B). Thus, based on the expected better resolution of biological age markers to explain age-related traits and the lack of relation of collagen parameters with chronological age in humans, we analyzed the collagen features in our groups of individuals of low versus high lipofuscin content. Individuals with high lipofuscin content have significantly higher values for collagen amount (median [IQR]: 2.77% [2.09%–4.23%]), clustering degree (median [IQR]: 12.91% [5.85%–15.01%]), and relative clustering (median [IQR]: 29.79‰ [15.98‰–49.37‰]) than the individuals with low lipofuscin content: median [IQR]: 0.72% [0.55%–1.20%] for collagen amount, median [IQR]: 3.99% [1.76%–7.04%] for the clustering degree, and median [IQR]: 4.06‰ [1.00‰–8.51‰] for the relative clustering (Figure 4C).

As per the spatial distribution of collagen aggregation, individuals with high lipofuscin content had nearly significantly higher values for the clustering distribution median (median [IQR]: 4.40% [3.16%–7.23%]) in comparison to individuals with low lipofuscin content (median [IQR]: 1.26% [0.10%–2.61%]), and significantly higher clustering distribution dispersion (median [IQR]: 10.35% [4.31%–12.31%] in comparison to individuals with low lipofuscin content (median [IQR]: 3.14% [1.48%–4.31%]) (Figure 4D). Thus, with increased biological age a higher degree of collagen aggregation and spatial dispersion of aggregation was found.

To further investigate the relationship between collagen features and both age markers, chronological age and lipofuscin, we performed Spearman correlation analysis with the full set of human samples (Figure 5). The percentages of collagen and lipofuscin were significantly correlated, while the correlation of each of them with chronological age was not significant in our cohort (Figure 5A). Although there is extensive literature evidence that collagen accumulates with age, our data for mid- to late-life age range indicated that collagen content correlated better with the age-pigment lipofuscin than with chronological age in humans (Figure 5A). The same is true for the relative clustering of collagen and its spatial distribution (Figures 5B–5D).

Collagen alterations associated with age play a major role in ventricular electrical propagation and pro-arrhythmicity

We next sought to understand how the amount, aggregation, and distribution of age-related collagen could influence the propagation of the electrical impulse in LV myocardium through *in silico* simulations. Therefore, we used the collagen and tissue masks obtained from the analysis of the SHG images from

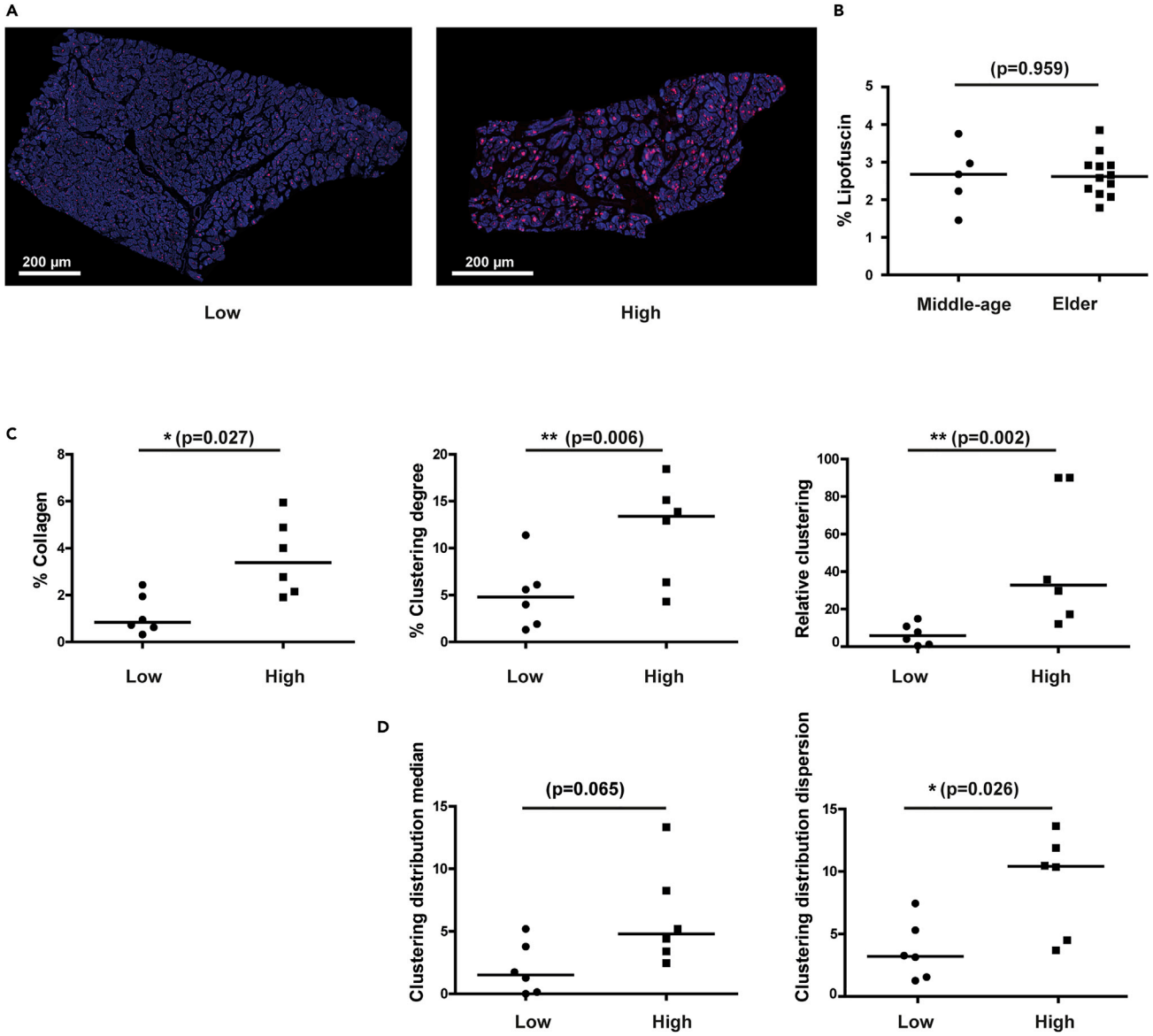

Figure 4. Quantification of lipofuscin amount in human LV sections

(A) Representative images of human LV tissue sections from individuals with low (left) and high (right) lipofuscin content.

(B) Lipofuscin content in middle-age versus elder humans.

(C) Comparison of collagen amount (left), clustering degree (middle), and relative clustering (right) between individuals with low and high lipofuscin content.

(D) Quantification of clustering distribution median (left) and clustering distribution dispersion (right) of collagen aggregations in middle-age to elder individuals.

In comparison between groups (B–D), black lines represent the median. Non-parametric Mann-Whitney test is used and p-values (p) are shown. See also Figure S3

donors to build two-dimensional computational tissue models in which each node of the corresponding tissue mesh was assigned collagen or myocardial properties based on these two masks (Figure 6A).

We used images from patients with five different degrees of collagen (1%, 2.5%, 4%, 5% and 6%). We built two-dimensional computational models and quantified the vulnerability window (VW) compared to the control condition (without fibrosis) and after varying the spatial distribution from patchy fibrosis, as observed in the patient, to diffuse fibrosis, simulating random scattering, but keeping constant the collagen percentage between both distributions (Figure 6B). Images presenting the spiral waves

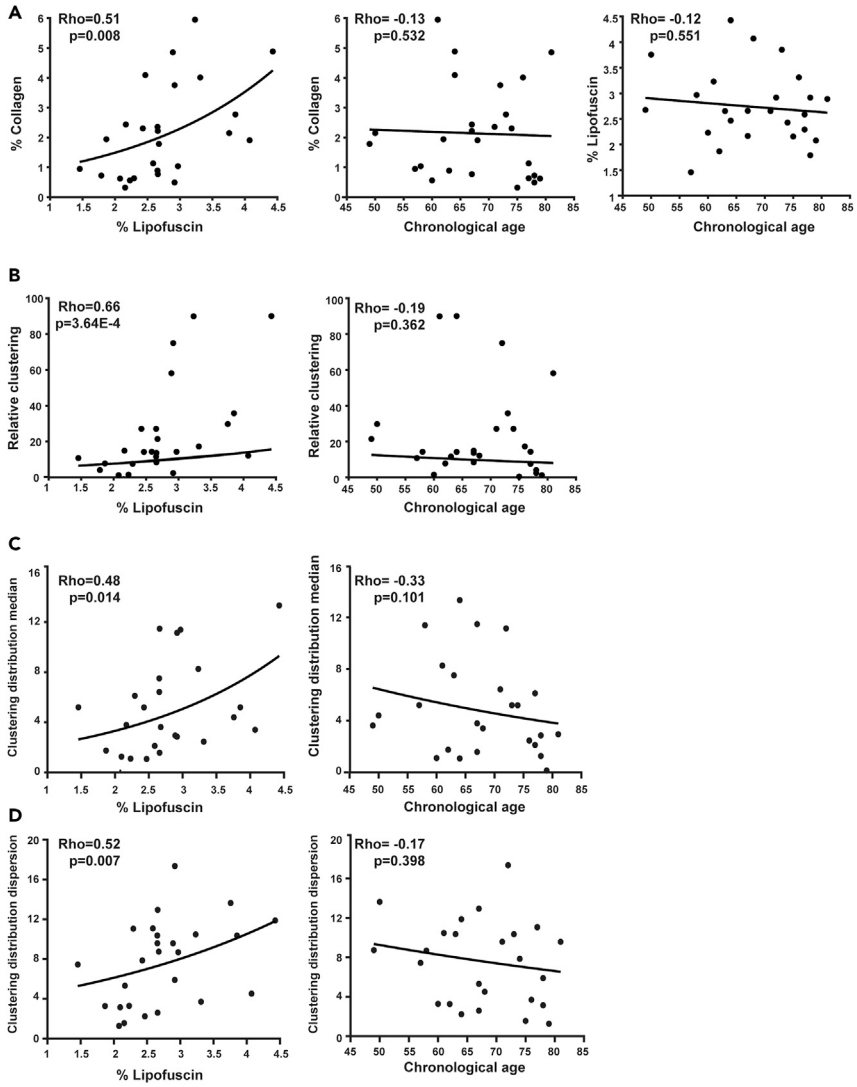

Figure 5. Correlation of collagen amount, aggregation and spatial distribution versus both age markers

(A) Correlation between collagen and lipofuscin (left), between collagen and chronological age (middle), and between chronological age and lipofuscin (right).

(B) Correlation between relative clustering and each of the two age markers, lipofuscin (left) and chronological age (right).

(C) Correlation between clustering distribution median and lipofuscin (left) or chronological age (right).

(D) Correlation between clustering distribution dispersion and lipofuscin (left) or chronological age (right).

For correlations, Spearman non-parametric test is used and correlation coefficients (Rho) and corresponding p-values (p) are shown.

generated for one of the patients under patchy and diffuse fibrosis are shown (Figure 6B). The VW is defined as the time interval where, if a premature stimulus is delivered, it can lead to a reentrant arrhythmia. For simulated tissues with diffuse fibrosis, we observed a low VW length for 1% fibrosis, which was increased for collagen percentages ranging from 2.5% to 6% (Table 2). For simulated tissues with patchy fibrosis, we observed high variability in the VW length, with no consistent pattern of VW increase or decrease with larger collagen percentage (Table 3). These results highlight not only the effect of collagen amount but also of its distribution on arrhythmia vulnerability.

DISCUSSION

In this study, we collected and processed SHG images of pig and human LV samples from living donors. We described an increasing tendency in LV myocardial collagen deposition with age in the two species. The degree

Table 2. Vulnerability window (VW) characteristics for the diffuse scenario (uniformly randomly distributed)

Diffuse	% Fibrosis	VW[a] length (ms)
Tissue 1	1%	7
Tissue 4	2.5%	16
Tissue 6	4%	14
Tissue 7	5%	15
Tissue 8	6%	18

[a]VW difference quantifies the VW length in a diffuse fibrosis scenario with respect to the control scenario.

of collagen clustering and its spatial dispersion increases from young age to adulthood, but not from adulthood to old age in pigs and not from middle-age to old age in humans. We showed that all the studied collagen features correlate with biological age better than with chronological age. Using computational modeling and simulation of two-dimensional human ventricular tissues based on patient-specific SHG images, we showed how age-induced changes in collagen content and organization can contribute to pro-arrhythmicity.

The tendency to higher LV collagen content in old versus young pigs agrees with the established association of increased collagen deposition with age in animal models (Horn and Trafford, 2016). Specifically in pigs, our results agree with reported larger degrees of interstitial fibrosis in the LV and septum in mini-pigs with Hutchinson–Gilford progeria syndrome as compared to controls (Dorado et al., 2019). In the human LV, we found a moderate trend toward higher collagen content in elder (median: 1.72%) versus middle-age (median: 1.04%) individuals. Despite extensive research in animal models, there is a paucity of studies in the literature quantifying changes in collagen percentage in the human LV with aging. One study using Picrosirius staining and polarized filters on autopsy samples from the esternocostal region of the LV showed increased collagen content in elder (67–87 years old, n = 6, mean: 5.92%) versus young (20–25 years old, n = 6, mean: 3.86%) individuals with no previous pathology (Gazoti Debessa et al., 2001). Similar results with comparable age ranges were described in another study using Picrosirius red staining too (Mendes et al., 2012). Our results, obtained with a more sensitive technique and automated quantification, are in line with these findings even if our collagen amounts are smaller, likely due to the higher specificity of SHG for collagen detection over histological techniques. Also, collagen III is likely to not be detected properly with our image acquisition setup due to its low-intensity SHG signal, but this would be systematic in our data. However, in the human age ranges analyzed here, such differences are not statistically significant, similarly to the comparison of adult and old pigs. Only when comparing to young animals, the age-related differences become borderline significant. Altogether, this study supports increased collagen deposition with advanced chronological age in both human and pig LV, which is accompanied by higher inter-individual variability in the elder.

Distinct forms of fibrosis exist that act through different mechanisms: replacement fibrosis, which repairs damaged areas found e.g. after myocardial infarction, or reactive fibrosis, a fine fibrosis that is generally present perivascularly or in the interstitium. Reactive interstitial fibrosis has a diffuse aspect while replacement and perivascular fibrosis are patchier. These types of fibrosis can coexist and classification of the predominant type of fibrosis is capital to develop potential curative treatments or to predict fibrosis-related arrhythmia risk (de Boer et al., 2019). The global increase in collagen deposition in pigs is chiefly accounted by non-clustered one (Figure 2D), thus diffuse interstitial fibrosis, but it is accompanied by raised patchy fibrosis that increases its spatial dispersion as the level of clustered collagen elevates. This collagen dynamics agree with what would be expected for a chronic fibrotic process like aging and with what is known from animal models (Biernacka and Frangogiannis, 2011). In the human LV, similarly to the porcine LV, most of the collagen is not clustered both for middle-age and elder groups and the relation between increased spatial dispersion and raising clustering is also verified. Our results are novel in quantifying the degree of LV fibrosis being clustered and non-clustered with age in humans and in a clinically relevant large animal model like the pig. The parallelism observed between humans and healthy farm pigs (particularly, middle-age and elder humans, and adult and old pigs) for all evaluated collagen features could experimentally support the use of pig to investigate the effects of LV fibrotic remodeling with natural aging.

Table 3. Vulnerability window (VW) characteristics for the patchy scenario (image-based) based on patient-specific images

Patchy	% Fibrosis	VW[a] length (ms)
Tissue 1	1%	0
Tissue 2	1%	1
Tissue 3	2.5%	8.5
Tissue 4	2.5%	14
Tissue 5	4%	3.5
Tissue 6	4%	16.5
Tissue 7	5%	9
Tissue 8	6%	16.5

[a]VW difference quantifies the VW length in a patchy fibrosis scenario with respect to the control scenario.

In humans, we observed high inter-individual variability in the collagen content in the analyzed age groups, but even higher in the elder group. Because all the biopsies were collected from the same LV region and transmural depth, regional differences are not expected to contribute to the observed variability. In addition, previous studies have shown similar collagen content among LV regions and from the inner to the outer layers of the LV wall in normal human hearts (Tanaka et al., 1986). Thus, we postulated that inter-individual differences in the aging rates could help to better explain the observed variability in the relationship between fibrosis and chronological age. We found that all the collagen parameters were more remarkably correlated with the lipofuscin percentage than with chronological age. Thus, the histological biological age better represents structural remodeling in the human LV as compared to chronological age. Unfortunately, we could not investigate this relationship in pigs since lipofuscin was not detectable by either autofluorescence or hematoxylin-eosin staining. Even if hematoxylin-eosin staining is not specific for lipofuscin detection, clear brown perinuclear aggregates could be observed in human samples but not in pig ones. Lipofuscin aggregates have been found in swine brain (Nanda and Getty, 1971), but, to the best of our knowledge, there are no reports indicating its presence in porcine LV myocardium. Thus, in humans, the use of lipofuscin as a biological indicator of age in middle-age to elder individuals is suggested as an improved descriptor of LV fibrotic remodeling as compared to chronological age.

Next, we investigated the role of age-induced accumulation of collagen in the LV in promoting cardiac arrhythmias, whose incidence is well known to increase in aged hearts, particularly from the sixth decade of life (Curtis et al., 2018; Lakatta and Levy, 2003; Segovia-Roldan et al., 2021). The association between increased fibrosis and arrhythmias, including ventricular tachycardia and ventricular fibrillation, has been well established in diseased hearts (Almaas et al., 2013; Morita et al., 2014; Shenasa, 2019; Sohns and Marrouche, 2020). This promotion occurs both by altering cardiac conduction and thus facilitating reentry as well as by modulating the formation of early afterdepolarizations leading to triggered activity (Karagueuzian, 2011). In aged hearts, fibrosis has been shown to act as a substrate that, together with a mild form of stress, can cause arrhythmias, which would not otherwise occur in non-fibrotic hearts subjected to the same stress (Karagueuzian, 2011; Spadaccio et al., 2015). It should be noted, however, that most of these studies on age-induced fibrosis and arrhythmias have been conducted in small animals, possibly due to the difficulty in obtaining human LV samples from non-diseased myocardium. Here, we used the results of our experimental characterization to feed computational models of ventricular electrophysiology by translating the tissue geometry and collagen amount and organization from the human LV samples into the 2D meshes used in the simulations. Although other studies have evaluated the effect of fibrosis amount and spatial scattering on ventricular electrophysiology by using different fibrosis distributions (Heikhmakhtiar et al., 2021), we built tissue models representative of a set of tissue geometries, collagen amounts, and distributions corresponding to our analyzed SHG images obtained from living donors rather than assigning generic collagen distributions not specific of individual patients. We found that, in the human LV, not only the total amount of fibrosis, but also its spatial distribution are fundamental factors in determining arrhythmia vulnerability, in accordance with previous investigations (Comtois and Nattel, 2011; Kawara et al., 2001; Kazbanov et al., 2016). In fact, when we simulated fibrosis in diffuse form and in the form of patches as in our SHG images, we found that the effects on VW were different for these two forms even if the total amount of fibrosis was kept constant. Our findings are in agreement with studies reporting an impact of intermediate, but not of very mild (below 4%) or severe (above 40%) fibrosis in arrhythmia

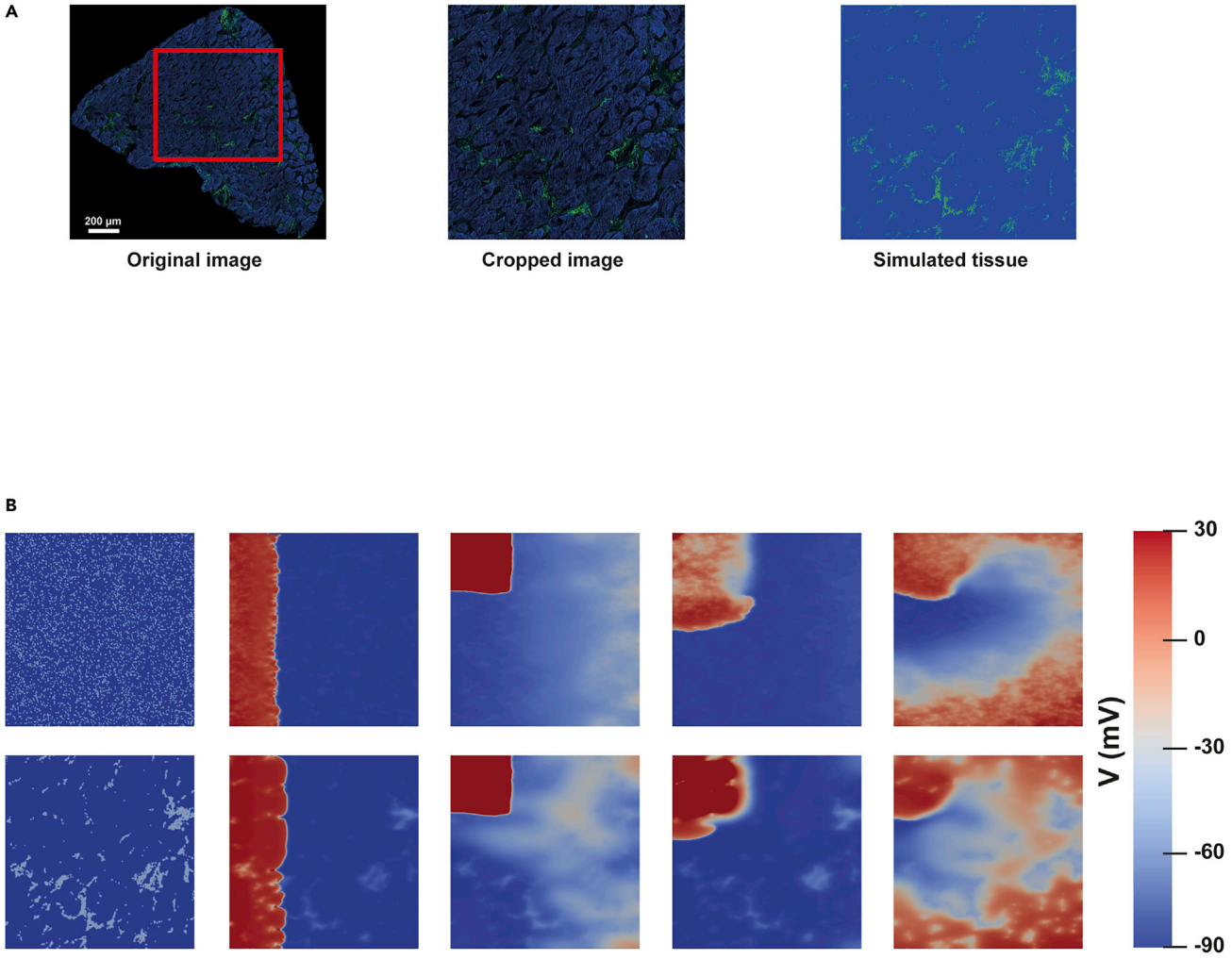

Figure 6. Assessment of vulnerability window (VW) increases in relation to age-related fibrosis in human LV samples

(A) Original image from a patient (left), cropped imaged selected for the simulation (middle) and merge image of collagen and tissue masks used in the simulation (right).

(B) Spiral wave generation with S1-S2 cross-stimulation protocol for cases of diffuse collagen distribution (top row) and patchy collagen distribution (bottom row).

propensity (Gomez et al., 2014; Morita et al., 2009; Ten Tusscher and Panfilov, 2007), even if we reported a substantial increase in VW length for fibrosis percentages above 2.5%.

In our realistic patchy fibrosis simulations, we observed high variability between tissues highlighting not only the effect of collagen amount, but also of its distribution on arrhythmia vulnerability. The differences between diffuse and patchy distribution, even if the collagen percentage was kept constant, underline the value of performing patient-specific simulations based on real distributions and not using generic collagen distributions that, although useful, can lead to partially different conclusions. Taken together, our study adds to previous evidence on the potential of LV myocardial fibrosis as an indicator of adverse pro-arrhythmic outcomes (de Jong et al., 2011; Karagueuzian, 2011; Morita et al., 2014) with particular emphasis in this study on age-associated effects in the human heart. Fibrosis characterization at microscopic levels, which remains so far very limited for the human LV, and the potential of the performed patient-specific computational simulations are major contributions from this work.

In conclusion, we have validated that collagen content, clustering and spatial distribution can be analyzed using SHG microscopy and automatic processing methods that avoid discrepancies between observers and yield higher specificity and resolution than cardiac imaging techniques used routinely. Even though

SHG cannot be used in the clinical context as an *in vivo* imaging tool, it has the potential to render new insights at the molecular and histological levels that could advance the medical practice. For example, as reported here, it is technically feasible to obtain transmural tissue biopsies from living donors where SHG in combination with lipofuscin content could aid in establishing basic features of age-related cardiac remodeling that, even if quantified by other methods, could eventually be used in patient management strategies. Although age-related collagen dynamics has limited relation with chronological age in mid-to-late life, we have shown that it is more closely related to lipofuscin, which highlights the use of biological age markers in age-associated cardiac fibrosis research, particularly in clinically relevant age ranges. By integrating the results of processing SHG images into *in silico* two-dimensional electrophysiological models, our tissue simulations show the value of collagen amount and distribution as risk indicators for cardiac arrhythmias. Additionally to the study on human LV tissues, our study highlights the pig as a suitable model of age-related LV structural remodeling over natural chronological aging.

Limitations of the study

Although this study showed the utility of LV biopsies from living donors to study age-related cardiac fibrosis and its contribution to cardiac arrhythmia generation, a limitation is the reduced number of human samples due to the difficulty in obtaining LV biopsies. Nevertheless, the number of employed samples is sensibly higher compared to that in other human studies (Gazoti Debessa et al., 2001; Kawara et al., 2001; Mendes et al., 2012).

Studies on LV tissues from living donors have the limitation that donors are not completely healthy. In this study, biopsies were collected from a region far from the areas irrigated by the obstructed artery in coronary patients. Besides, we conducted parallel analysis in healthy porcine samples and we found that collagen content and clustering characteristics were similar between these two species. This highlights the role of age in collagen dynamics beyond potential disease-induced effects in humans.

STAR★METHODS

Detailed methods are provided in the online version of this paper and include the following:

- KEY RESOURCES TABLE
- RESOURCE AVAILABILITY
  - Lead contact
  - Materials availability
  - Data and code availability
- EXPERIMENTAL MODEL AND SUBJECT DETAILS
  - Ethical approvals and patients clinical information
- METHOD DETAILS
  - Collection and processing of left ventricular tissues
  - Non-linear optical microscopy
  - Masson's trichrome staining
  - Image processing for evaluation of collagen amount, aggregation and spatial distribution
  - Image processing for lipofuscin quantification
  - Inter-observer agreement
  - Simulation of ventricular electrical activity as a function of collagen characteristics
- QUANTIFICATION AND STATISTICAL ANALYSIS

SUPPLEMENTAL INFORMATION

Supplemental information can be found online at https://doi.org/10.1016/j.isci.2022.103822

ACKNOWLEDGMENTS

This work was supported by Ministerio de Ciencia e Innovación (Spain) (PID2019-105674RB-I00), by Gobierno de Aragón (LMP94_21) and (LMP128_21), by the European Research Council through grant ERC-StG 638284 and by European Social Fund and by Gobierno de Aragón (Reference Group BSICoS T39-20R) cofunded by FEDER 2014–2020 "Building Europe from Aragon". L.G-M was supported by a predoctoral fellowship from the Departamento de Ciencia, Universidad y Sociedad del Conocimiento from the Gobierno de Aragón 2016–2020 cofounded by Programa Operativo del Fondo Social Europeo Aragón (C150/2016), EMBO Short-Term fellowship (7710), and Ibercaja-CAI Estancias de Investigación IT18/18.

Authors would like to acknowledge the Experimental Surgery Service of Aragon Health Sciences Institute (CIBA, Zaragoza, Spain), Mercazaragoza slaughterhouse (Zaragoza, Spain), and The Pink Pig slaughterhouse (Zuera, Spain) for their collaboration in the collection of young, adult, and boar tissue specimens, respectively.

AUTHORS CONTRIBUTIONS

L.G-M., L.O., and E.P. conceived the study. L.O. and E.P. supervised the study. L.G-M., N.S., M.P-Z., K.M., SD, E.W., and R.D performed experiments and analyzed the data. M.P-Z., K.M., and E.D. designed the software for image analysis. K.M. and L.G-M performed the simulations. J.M.V-G., P.C.F-R., J.F-M., M.V-S., M.M-A., J.F.S-B., J.A.B-M., F.J.M-S., A.S.V-N., and C.B-C. collected the human LV samples. A.O-V. processed the human LV samples. M.*P. and* L.L. contributed to the histological analysis. L.G-M. wrote the manuscript with contributions by L.O. and E.P., and all the authors carefully reviewed the data and the manuscript.

DECLARATION OF INTERESTS

The authors declare no competing interests.

Received: June 1, 2021
Revised: December 14, 2021
Accepted: January 25, 2022
Published: February 18, 2022

REFERENCES

Almaas, V.M., Haugaa, K.H., Strøm, E.H., Scott, H., Dahl, C.P., Leren, T.P., Geiran, O.R., Endresen, K., Edvardsen, T., Aakhus, S., et al. (2013). Increased amount of interstitial fibrosis predicts ventricular arrhythmias, and is associated with reduced myocardial septal function in patients with obstructive hypertrophic cardiomyopathy. Europace *15*, 1319–1327.

Ávila, F.J., and Bueno, J.M. (2015). Analysis and quantification of collagen organization with the structure tensor in second harmonic microscopy images of ocular tissues. Appl. Opt. *54*, 9848–9854.

Biernacka, A., and Frangogiannis, N.G. (2011). Aging and cardiac fibrosis. Aging Dis. *2*, 158–173.

Brunk, U.T., and Terman, A. (2002). Lipofuscin: mechanisms of age-related accumulation and influence on cell function. Free Radic. Biol. Med. *33*, 611–619.

Burlew, B.S., and Weber, K.T. (2002). Cardiac fibrosis as a cause of diastolic dysfunction. Herz *27*, 92–98.

Büttner, P., Galli, R., Husser, D., and Bollmann, A. (2018). Label-free imaging of myocardial remodeling in atrial fibrillation using nonlinear optical microscopy: a feasibility study. J. Atr. Fibrillation *10*, 3–7.

Chiu, Y.-W., Lo, M.T., Tsai, M.-R., Chang, Y.-C., Hsu, R.-B., Yu, H.-Y., Sun, C.-K., and Ho, Y.-L. (2010). Applying harmonic optical microscopy for spatial alignment of atrial collagen fibers. PLoS One *5*, 1–9.

Comtois, P., and Nattel, S. (2011). Interactions between cardiac fibrosis spatial pattern and ionic remodeling on electrical wave propagation. Annu. Int. Conf. IEEE Eng. Med. Biol. Soc. *2011*, 4669–4672.

Curtis, A.B., Karki, R., Hattoum, A., and Sharma, U.C. (2018). Arrhythmias in patients ≥80 years of age: pathophysiology, management, and outcomes. J. Am. Coll. Cardiol. *71*, 2041–2057.

de Bakker, J.M., van Capelle, F.J., Janse, M.J., Tasseron, S., Vermeulen, J.T., de Jonge, N., and Lahpor, J.R. (1993). Slow conduction in the infarcted human heart. "Zigzag" course of activation. Circulation *88*, 915–926.

de Boer, R.A., De Keulenaer, G., Bauersachs, J., Brutsaert, D., Cleland, J.G., Diez, J., Du, X.-J., Ford, P., Heinzel, F.R., Lipson, K.E., et al. (2019). Towards better definition, quantification and treatment of fibrosis in heart failure. a scientific roadmap by the committee of translational research of the heart failure association (hfa) of the european society of cardiology. Eur. J. Heart Fail. *21*, 272–285.

de Jong, S., van Veen, T.A.B., van Rijen, H.V.M., and de Bakker, J.M.T. (2011). Fibrosis and cardiac arrhythmias. J. Cardiovasc. Pahrmacology *57*, 630–638.

Disertori, M., Masè, M., and Ravelli, F. (2017). Myocardial fibrosis predicts ventricular tachyarrhythmias. Trends Cardiovasc. Med. *27*, 363–372.

Dorado, B., Pløen, G.G., Barettino, A., Macías, A., Gonzalo, P., Andrés-Manzano, M.J., González-Gómez, C., Galán-Arriola, C., Alfonso, J.M., Lobo, M., et al. (2019). Generation and characterization of a novel knockin minipig model of Hutchinson-Gilford progeria syndrome. Cell Discov *5*, 16.

Gazoti Debessa, C.R., Mesiano Maifrino, L.B., and Rodrigues de Souza, R. (2001). Age related changes of the collagen network of the human heart. Mech. Ageing Dev. *122*, 1049–1058.

Gomez, J.F., Cardona, K., Martinez, L., Saiz, J., and Trenor, B. (2014). Electrophysiological and structural remodeling in heart failure modulate arrhythmogenesis. 2D simulation study. PLoS One *9*, e103273.

Hassan, S., Barrett, C.J., and Crossman, D.J. (2020). Imaging tools for assessment of myocardial fibrosis in humans: the need for greater detail. Biophys. Rev. *12*, 969–987.

Heikhmakhtiar, A.K., Tekle, A.A., and Lim, K.M. (2021). Influence of fibrosis amount and patterns on ventricular arrhythmogenesis and pumping efficacy: computational study. Front. Physiol. *12*, 644473.

Horn, M.A., and Trafford, A.W. (2016). Aging and the cardiac collagen matrix: novel mediators of fibrotic remodelling. J. Mol. Cell. Cardiol. *93*, 175–185.

Kakimoto, Y., Okada, C., Kawabe, N., Sasaki, A., Tsukamoto, H., Nagao, R., and Osawa, M. (2019). Myocardial lipofuscin accumulation in ageing and sudden cardiac death. Sci. Rep. *9*, 1–8.

Karagueuzian, H.S. (2011). Targeting cardiac fibrosis : a new frontier in antiarrhythmic therapy? Am. J. Cardiovasc. Dis. *1*, 101–109.

Kawara, T., Derksen, R., de Groot, J.R., Coronel, R., Tasseron, S., Linnenbank, A.C., Hauer, R.N.W., Kirkels, H., Janse, M.J., and de Bakker, J.M.T. (2001). Activation delay after premature stimulation in chronically diseased human myocardium relates to the architecture of interstitial fibrosis. Circulation *104*, 3069–3075.

Kazbanov, I.V., ten Tusscher, K.H.W.J., and Panfilov, A.V. (2016). Effects of heterogeneous diffuse fibrosis on arrhythmia dynamics and mechanism. Sci. Rep. *6*, 1–14.

Lakatta, E.G., and Levy, D. (2003). Arterial and cardiac aging: major shareholders in cardiovascular disease enterprises part II: the

aging heart in health: links to heart disease. Circulation *107*, 346–354.

Liu, C.-Y., Liu, Y.-C., Wu, C., Armstrong, A., Volpe, G.J., van der Geest, R.J., Liu, Y., Hundley, W.G., Gomes, A.S., Liu, S., et al. (2013). Evaluation of age-related interstitial myocardial fibrosis with cardiac magnetic resonance contrast-enhanced T1 mapping multi-ethnic study of atherosclerosis (MESA). J. Am. Coll. Cardiol. *62*, 1280–1287.

Liu, Y., Keikhosravi, A., Mehta, G.S., Drifka, C.R., and Eliceiri, K.W. (2017). Methods for quantifying fibrillar collagen alignment. Methods Mol. Biol. *1627*, 429–451.

MacCannell, K.A., Bazzazi, H., Chilton, L., Shibukawa, Y., Clark, R.B., and Giles, W.R. (2007). A mathematical model of electrotonic interactions between ventricular myocytes and fibroblasts. Biophys. J. *92*, 4121–4132.

Mendes, A.B.L., Ferro, M., Rodrigues, B., Souza, M.R. de, Araujo, R.C., and Souza, R.R. de (2012). Quantification of left ventricular myocardial collagen system in children, young adults, and the elderly. Medicina (B. Aires). *72*, 216–220.

Morita, N., Mandel, W.J., Kobayashi, Y., and Karagueuzian, H.S. (2014). Cardiac fibrosis as a determinant of ventricular tachyarrhythmias. J. Arrhythmia *30*, 389–394.

Morita, N., Sovari, A.A., Xie, Y., Fishbein, M.C., Mandel, W.J., Garfinkel, A., Lin, S.-F., Chen, P.-S., Xie, L.-H., Chen, F., et al. (2009). Increased susceptibility of aged hearts to ventricular fibrillation during oxidative stress. Am. J. Physiol. Heart Circ. Physiol. *297*, H1594–H1605.

Mostaço-Guidolin, L., Rosin, N.L., and Hackett, T.-L. (2017). Imaging collagen in scar tissue: developments in second harmonic generation microscopy for biomedical applications. Int. J. Mol. Sci. *18*, 1772.

Mountris, K.A., and Pueyo, E. (2020). The radial point interpolation mixed collocation method for the solution of transient diffusion problems. Eng. Anal. Bound. Elem. *121*, 207–216.

Mountris, K.A., and Pueyo, E. (2021a). Cardiac electrophysiology meshfree modeling through the mixed collocation method. arXiv, Preprint at: arXiv:2110.06671.

Mountris, K.A., and Pueyo, E. (2021b). A dual adaptive explicit time integration algorithm for efficiently solving the cardiac monodomain equation. Int. J. Numer. Method. Biomed. Eng. *37*, e3461.

Nanda, B.S., and Getty, R. (1971). Lipofuscin pigment in the nervous system of aging pig. Exp. Gerontol. *6*, 447–452.

O'Hara, T., Virág, L., Varró, A., and Rudy, Y. (2011). Simulation of the undiseased human cardiac ventricular action potential: model formulation and experimental validation. PLoS Comput. Biol. *7*, e1002061.

Oliván-Viguera, A., Pérez-Zabalza, M., García-Mendívil, L., Mountris, K.A., Orós-Rodrigo, S., Ramos-Marquès, E., Vallejo-Gil, J.M., Fresneda-Roldán, P.C., Fañanás-Mastral, J., Vázquez-Sancho, M., et al. (2020). Minimally invasive system to reliably characterize ventricular electrophysiology from living donors. Sci. Rep. *10*, 19941.

Perbellini, F., Liu, A.K.L., Watson, S.A., Bardi, I., Rothery, S.M., and Terracciano, C.M. (2017). Free-of-acrylamide SDS-based tissue clearing (FASTClear) for three dimensional visualization of myocardial tissue. Sci. Rep. *7*, 5188.

Perbellini, F., Watson, S.A., Scigliano, M., Alayoubi, S., Tkach, S., Bardi, I., Quaife, N., Kane, C., Dufton, N.P., Simon, A., et al. (2018). Investigation of cardiac fibroblasts using myocardial slices. Cardiovasc. Res. *114*, 77–89.

Ramos-Marquès, E., García-Mendívil, L., Pérez-Zabalza, M., Santander-Badules, H., Srinivasan, S., Oliveros, J.C., Torres-Pérez, R., Cebollada, A., Vallejo-Gil, J.M., Fresneda-Roldán, P.C., et al. (2021). Chronological and biological aging of the human left ventricular myocardium: analysis of microRNAs contribution. Aging Cell. Jul *20*, e13383.

Schneider, C.A., Rasband, W.S., and Eliceiri, K.W. (2012). NIH image to imageJ: 25 years of image analysis. Nat. Methods *9*, 671–675.

Segovia-Roldan, M., Diez, E.R., and Pueyo, E. (2021). Melatonin to rescue the aged heart: antiarrhythmic and antioxidant benefits. Oxid. Med. Cell. Longev. *2021*, 8876792.

Shenasa, M. (2019). Fibrosis and ventricular arrhythmogenesis: role of cardiac MRI. Card. Electrophysiol. Clin. *11*, 551–562.

Sohns, C., and Marrouche, N.F. (2020). Atrial fibrillation and cardiac fibrosis. Eur. Heart J. *41*, 1123–1131.

Spadaccio, C., Rainer, A., Mozetic, P., Trombetta, M., Dion, R.A., Barbato, R., Nappi, F., and Chello, M. (2015). The role of extracellular matrix in age-related conduction disorders: a forgotten player? J. Geriatr. Cardiol. *12*, 76–82.

Strupler, M., Pena, A.-M., Hernest, M., Tharaux, P.-L., Martin, J.-L., Beaurepaire, E., and Schanne-Klein, M.-C. (2007). Second harmonic imaging and scoring of collagen in fibrotic tissues. Opt. Express *15*, 4054–4065.

Suk, T., Edwards, C., Hart, H., and Christiansen, J.P. (2008). Myocardial scar detected by contrast-enhanced cardiac magnetic resonance imaging is associated with ventricular tachycardia in hypertrophic cardiomyopathy patients. Heart Lung Circ. *17*, 370–374.

Tanaka, M., Fujiwara, H., Onodera, T., Wu, D.J., Hamashima, Y., and Kawai, C. (1986). Quantitative analysis of myocardial fibrosis in normals, hypertensive hearts, and hypertrophic cardiomyopathy. Br. Heart J. *55*, 575–581.

Ten Tusscher, K.H.W.J., and Panfilov, A.V. (2007). Influence of diffuse fibrosis on wave propagation in human ventricular tissue. Europace *9*, vi38–45.

Tilbury, K., Hocker, J., Wen, B.L., Sandbo, N., Singh, V., and Campagnola, P.J. (2014). Second harmonic generation microscopy analysis of extracellular matrix changes in human idiopathic pulmonary fibrosis. J. Biomed. Opt. *19*, 86014.

Tsai, M.-R., Chiu, Y.-W., Lo, M.T., and Sun, C.-K. (2010). Second-harmonic generation imaging of collagen fibers in myocardium for atrial fibrillation diagnosis. J. Biomed. Opt. *15*, 26002.

Williams, R.M., Zipfel, W.R., and Webb, W.W. (2005). Interpreting second-harmonic generation images of collagen I fibrils. Biophys. J. *88*, 1377–1386.

STAR★METHODS

KEY RESOURCES TABLE

REAGENT or RESOURCE	SOURCE	IDENTIFIER
Software and algorithms		
Zen blue 2.5	Carl Zeiss	https://www.zeiss.com/microscopy/int/products/microscope-software/zen-lite.html
ImageJ 1.53k	NIH	https://imagej.net/
MATLAB 2020b	MathWorks	https://es.mathworks.com/products/matlab.html
ELECTRA 0.4.5	In-house cardiac electrophysiology solver	https://www.mountris.org/cxx

RESOURCE AVAILABILITY

Lead contact

Further information should be directed to and will be fulfilled by the lead contact Dr. Laura Ordovás (lordovas@unizar.es).

Materials availability

This study did not generate new unique reagents.

Data and code availability

- All data reported in this paper will be shared by the lead contact upon request.
- Any additional information required to reanalyze the data reported in this paper is available from the lead contact upon request.

EXPERIMENTAL MODEL AND SUBJECT DETAILS

Ethical approvals and patients clinical information

All animal experiments complied with the regulations of the local animal welfare committee for the care and use of experimental animals and were approved by local ethics authorities (Ethics Committee on Animal Experimentation, CEAEA, of the University of Zaragoza). All animal procedures conformed to the guidelines from Directive (2010)/63/EU of the European Parliament on the protection of animals used for scientific purposes.

Collection and analysis of human LV samples conformed to the principles outlined in the Declaration of Helsinki and were approved by the local ethics committee (CEICA, reference number PI17/0023), with all patients giving written informed consent before surgery and prior to their inclusion in the study. The clinical characteristics of the patients are summarized in Table 1.

METHOD DETAILS

Collection and processing of left ventricular tissues

Pig transmural LV tissue specimens were collected from young female pigs (12–16 weeks old, 35 kg, n = 7) at the Experimental Surgery Service of the Biomedical Research Center of Aragón (CIBA, Zaragoza, Spain), adult male and female pigs (6 months, 110 kg, n = 8) at Mercazaragoza slaughterhouse (Zaragoza, Spain) and boars (4–5 years old, 300 kg, n = 11) at The Pink Pig slaughterhouse (Zuera, Spain). The samples were obtained 10–15 minutes after the sacrifice using a disposable 14 G tru-cut biopsy needle (Bard Mission 1410MS, Bard).

Human transmural LV tissue specimens were collected at Hospital Universitario Miguel Servet (Zaragoza, Spain) from patients older than 18 years old undergoing valve replacement surgery or coronary artery bypass, having all of them preserved systolic function and absence of ventricular hypertrophy or dilated cardiomyopathy (n = 26). The clinical characteristics of the patients are summarized in Table 1. The samples were obtained with a 14 G tru-cut biopsy needle during cardiac arrest, immediately after the patient was

placed on cardiopulmonary bypass, from an area of the anterior wall of the LV, near the base of the heart, with no evidence of ischemia or any other macroscopic pathology (Oliván-Viguera et al., 2020). For comparison purposes, two age groups were established: middle-age (54.8 ± 4.97, n = 5) and elder (75.92 ± 3.0, n = 12). For correlation analysis, samples from all the individuals were used.

Immediately upon collection, tissue specimens were placed in freshly prepared ice-cold preoxygenated 30mM BDM-Tyrode's solution as described in (Oliván-Viguera et al., 2020). The specimens were then transferred to 4% paraformaldehyde fixative solution for 1h at 4°C and stored in 0.01% sodium-azide in PBS at 4°C until embedded in paraffin blocks. Tissue sections of 5 μm were mounted on microscope slides for SHG analysis.

Non-linear optical microscopy

SHG microscopy was used to quantitatively assess collagen deposition in LV tissue samples combined with two-photon excitation fluorescence microscopy to detect cellular and lipofuscin autofluorescence. A Zeiss LSM 880 (Carl Zeiss, AG, Jena, Germany) mounted on the rear port of an Axio Observer.Z1 stand was employed. Excitation was provided by a femtosecond pulsed laser (Mai Tai DeepSee, Spectra-Physics, CA, USA) tuned to a central wavelength of 810 nm, passed through an acousto-optic modulator and coupled into the LSM880 scanhead. The laser light was directed to the sample using a 760 nm shortpass dichroic mirror (MBS 760+) and ~80 mW average power was focused on the sample through a plan-apochromat 20x objective (NA 0.8, Carl Zeiss, AG, Jena, Germany). Throughout the experiments, we acquired images with a bit depth of 16 bits, used a constant pixel dwell time of 4.48 μs, unidirectional scanning and a zoom factor of 1.3 that resulted in a constant square pixel size of 170 × 170 nm when imaging with a resolution of 1872 by 1872 pixels to fulfill Nyquist criterion. For samples larger than a single field of view, we performed a tile scan to cover the complete sample with 10% overlap between the tiles to enable a seamless stitching of these tiles.

To facilitate fast acquisitions of large samples, three channels were simultaneously recorded with a fully opened pinhole, using the 34 channel QUASAR spectral detector unit (2 PMTs (Ch1 and Ch2) + 32 channel GaAsP array (ChS1)). SHG signal was detected in Ch1 (PMT, wavelength range 380–420 nm, detector gain 750, digital offset 256). Cellular autofluorescence was detected using ChS1 (32 channel GaAsP array, wavelength range 500–552 nm, detector gain 680, digital offset 64). Lipofuscin autofluorescence was detected in Ch2 (PMT, wavelength range 650–735 nm, detector gain 750, digital offset 256).

Masson's trichrome staining

Masson's trichrome staining was performed after SHG. Briefly, 5-μm-thick deparaffinized sections were stained with hematoxylin for 5 minutes. The slides were subsequently washed and, following 5 minutes of ponceau/fucsine solution and washing, phosphomolybdic acid 1% was applied for 5 minutes. Collagen was stained with Aniline Blue Solution for 8 minutes, following which phosphomolybdic acid 1% was applied again for 5 minutes. Finally, the sections were rinsed in acetic acid 1% for 1 minute, before dehydrating and mounting in DPX mounting medium. Slides were left to dry overnight and were evaluated using a Leica DM5000B microscope (Leica Microsystems, Wetzlar, Germany).

Image processing for evaluation of collagen amount, aggregation and spatial distribution

Original images (czi format) were exported as 16-bit tiff images using Zen blue software (Carl Zeiss, Jena, Germany), with each detection channel in a different channel. Images were processed for automatic brightness scaling using ImageJ (Schneider et al., 2012) and to remove isolated image segments, e.g. fluorescence artifacts or areas of clear perivascular fibrosis, before the quantitative analysis.

An in-house MATLAB v2020b user interface was developed to characterize the amount and distribution of collagen in the collected SHG microscopy data. From the 16-bit TIFF image, myocardial tissue (blue channel) and SHG signal (green channel) were extracted and converted into gray-level images. A binarization filter was applied to each of these gray-level images to generate binary masks for both myocardial tissue and SHG signal. Empty spaces in the myocardial tissue mask with less than 20 pixels were filled, and tissue segments with less than 15 pixels were associated with artifacts and discarded. For the SHG binary mask, isolated regions with less than 15 pixels were identified as correspondent with noise artifacts and were removed. SHG signal contained both myosin and collagen signals, being collagen the SHG signal that

does not colocalize with the myocardial tissue. This lack of colocalization was used to obtain the collagen mask from the SHG mask (Figure 1).

From the myocardial tissue and collagen masks, the percentage of collagen, P_c, was estimated as the number of activated pixels in the collagen mask (N_c) divided by the sum of activated pixels in the myocardial tissue (N_m) and the collagen masks:

$$P_c = \frac{Nc}{Nc + Nm} 100$$

From the collagen mask, the global clustering degree was calculated as the number of collagen pixels surrounded by collagen pixels in a circle of 2-pixel radius divided by the total number of collagen pixels. Additionally, a relative clustering measure was estimated as the product of percentages of collagen and clustering degree and it was expressed as per ten thousand (‱).

Furthermore, the spatial distribution of collagen clusters was obtained by windowing the collagen mask into 500 × 500 pixel subimages and calculating the collagen clustering in each of these subimages. An additional filter was applied to set a minimum number of pixels in any given subimage for it to be included in the analysis, and the threshold was set to 200 pixels. For the histogram of clustering degrees in all subimages of an image, we calculated the clustering distribution median, calculated as the median of the distribution, and the clustering distribution dispersion, estimated as the interquartile range of the distribution.

The pixel radius for global clustering, the window size for the spatial distribution of collagen clustering and the threshold for subimage acceptance were determined empirically. A 2-pixel radius, a window of 500 × 500 pixels and a threshold of 200 pixels were found to be adequate for evaluation of global collagen aggregation and its spatial distribution.

The reason for choosing a radius of 2 pixels was that clustering analysis using a smaller radius (radius of 1 pixel) led to almost every pixel of collagen being recognized as a cluster itself; with higher radius values (radius of 3-4-5 pixels), many collagen aggregates were not detected. The 2-pixel radius was the one more faithfully detecting grouped collagen pixels versus finely scattered one without losing small collagen aggregates. For spatial distribution analysis, we chose the area of sub-images to be 500 × 500 pixels since we observed to best fit the rationale of retrieving a sufficient amount of frames in all kind of tissue sections (big and small) that are large enough to avoid leaving tissue areas unconsidered due to low pixel count or, on the contrary, to reduce the analysis to just a few frames that will not capture distribution differences. The threshold for a minimum pixel amount in a subimage to be included in the distribution analysis was set to 200 pixels to avoid including isolated pixels in the quantification.

Image processing for lipofuscin quantification

The percentage of lipofuscin (P_l) was calculated as the amount of activated pixels in the lipofuscin mask (N_l) divided by the activated pixels in the myocardial tissue mask (N_m).

$$P_l = \frac{Nl}{Nm} 100$$

The image processing method to determine the percentage of lipofuscin is shown in Figure S3.

Inter-observer agreement

All image processing analysis was performed by two independent observers. To compare the results obtained by the two observers, Bland-Altman plots were obtained. For all quantifications, the level of agreement between the two observers, both in pig (Figure S1) and in human samples (Figure S2), was reported.

Simulation of ventricular electrical activity as a function of collagen characteristics

To assess the impact of the amount and distribution of collagen in cardiac action potential propagation, we built two-dimensional computational tissue models of human ventricular electrophysiology representative of a set of the analyzed tissues. Specifically, we took eight LV tissue sections from patients with ages ranging from 58 to 81 years old. and we merged the myocardial and collagen masks generated as described above. From this merged image, we took a square in each case to avoid possible effects on arrhythmia vulnerability associated with tissue geometry. These square images were resized to reduce

the number of pixels and, thus, alleviate the computational cost of the simulations. The obtained images were subsequently converted into quadrilateral meshes by assigning a quadrilateral element to each pixel of the image. For each mesh, the pixel size was rescaled to obtain 5 × 5 cm^2 simulated tissues.

The vertices of the mesh elements corresponding to collagen pixels were assigned the label "fibrotic" and their electrophysiology was represented by the MacCannell model of mammalian ventricular fibroblasts (MacCannell et al., 2007). The rest of vertices were assigned the label "myocardial" and their electrophysiology was described by the O'Hara-Rudy model of human ventricular cardiomyocytes (O'Hara et al., 2011). The longitudinal conductivity in the myocardial region was set to 0.13 mS/cm, while the transverse-to-longitudinal conductivity ratio was set to 0.25. In the fibrotic region, the conductivity values were three times lower than in the myocardial region.

The effect of fibrosis on spiral wave generation was investigated by applying an S1-S2 cross stimulation protocol (Mountris and Pueyo 2021a), with a sequence of periodic S1 stimuli followed by an extra stimulus S2 to assess pro-arrhythmicity due to the interaction of the S2 stimulus wave front with the S1 stimulus wave tail. In a first set of simulations, the S1 stimuli were applied at the left side of the tissue at t_{S1} = 50 ms, with duration t_d = 2 ms, period t_T = 1 s and amplitude A equal to twice the diastolic threshold. The S2 stimulus was applied on a patch region at the top left corner of the tissue with the same values of t_d and A as for the S1 stimulus. In a second set of simulations, the S1 stimuli were applied on the right side of the tissue and the S2 stimulus was applied at the top right corner. The stimulus time was varied to compute the vulnerability window (VW), defined as the time interval during which the S1-S2 interaction leads to the generation of a sustained spiral wave. The length of the VW was calculated, individually for each tissue, as the average of the VW lengths computed from the first and the second set of simulations.

To assess the effect of collagen amount on VW, simulations were conducted for each of the eight selected tissues under both control conditions (i.e. no collagen in the tissue) and fibrotic conditions (i.e. with the distribution of collagen as derived from processing the tissue images). When simulating control conditions, the O'Hara-Rudy action potential model was assigned to all vertices of the tissue mesh. To assess vulnerability to reentry, continuous tissues were simulated by filling any holes in them. To keep the percentages of collagen similar to the ones before filling the holes, i.e. as quantified in the original patients' images, we added collagen to the filled regions according to a uniform random distribution to guarantee that those regions had the same collagen percentage as the original image.

To assess the effect of collagen distribution on VW, simulations were run for a patchy fibrosis configuration (with the image-derived collagen distribution as described in the previous paragraph) and for a diffuse fibrosis configuration (with collagen assumed to be uniformly randomly distributed across the tissue). For each tissue, the patchy and diffuse configurations contained the same percentage of collagen, measured as the ratio of mesh elements labeled as fibrotic divided by the total number of mesh elements.

Simulations were performed using ELECTRA which is an in-house cardiac electrophysiology solver implementing the Finite Element Method and Meshless methods (Mountris and Pueyo, 2020, 2021a) for the solution of the cardiac monodomain model (Mountris and Pueyo, 2020, 2021b). In this work, the dual-adaptive explicit integration algorithm (Mountris and Pueyo, 2021b) was used to efficiently solve the monodomain model.

QUANTIFICATION AND STATISTICAL ANALYSIS

Mann-Whitney test was used to assess differences between two independent groups. Spearman correlation analysis was used to test the strength and direction of association between two variables. The significance threshold was established at p-value = 0.05 for both Mann-Whitney and Spearman correlation. The p-values for Mann-Whitney comparisons and the p-values and correlation coefficients for Spearman correlations are shown in every figure. Unless otherwise indicated, data are presented as median [interquartile range (IQR)]. All statistical analysis were performed with MATLAB v2020b.